BIOCHEMISTRY
including biophysical chemistry & molecular biology

RAPID REPORT

pubs.acs.org/biochemistry

Acoustically Mounted Microcrystals Yield High-Resolution X-ray Structures

Alexei S. Soares,[†,*] Matthew A. Engel,[‡,§] Richard Stearns,[∥] Sammy Datwani,[∥] Joe Olechno,[∥] Richard Ellson,[∥] John M. Skinner,[†] Marc Allaire,[*,‡] and Allen M. Orville[*,†]

[†]Biology Department, Brookhaven National Laboratory, Upton, New York 11973-5000, United States

[‡]National Synchrotron Light Source, Brookhaven National Laboratory, Upton, New York 11973-5000, United States

[§]Department of Biomedical Engineering, Stony Brook University, Stony Brook, New York 11794-2580, United States

[∥]Labcyte Inc., 1190 Borregas Avenue, Sunnyvale, California 94089, United States

Supporting Information

ABSTRACT: We demonstrate a general strategy for determining structures from showers of microcrystals. It uses acoustic droplet ejection to transfer 2.5 nL droplets from the surface of microcrystal slurries, through the air, onto mounting micromesh pins. Individual microcrystals are located by raster-scanning a several-micrometer X-ray beam across the cryocooled micromeshes. X-ray diffraction data sets merged from several micrometer-sized crystals are used to determine 1.8 Á resolution crystal structures.

Microcrystals measuring only a few micrometers along an edge are often easy to obtain, even from viruses, membrane proteins, protein−protein complexes, or protein−nucleic acid complexes. They are ubiquitous but difficult to use because they are too small to yield a suitable diffraction pattern with conventional macromolecular crystallography (MX). Fortunately, advances in X-ray sources at third-generation synchrotrons and free electron lasers (FEL)[1,2] are rapidly reducing the sample size[3−5] and exposure time required for atomic-level crystal structure determination.[6,7] As an example, consider that an MX beamline at National Synchrotron Light Source II (NSLS-II) currently under construction at the Brookhaven National Laboratory will produce a 1 μm diameter X-ray beam with sufficient intensity that a similarly sized protein crystal is projected to reach its maximum dose limit in as little as 5 ms.[8] However, as the crystal size is reduced, so is the signal relative to the noise in the X-ray diffraction data. Consequently, an essential strategy for improving the signal-to-noise ratio is to reduce the background scattering, especially from the mother liquor surrounding a micrometer-sized crystal. Unfortunately, removing all the excess mother liquor is very difficult as the crystal size approaches a few cubic micrometers. Therefore, robust new strategies must be developed to manipulate microcrystals for structure determination.

To address this critical gap, we are developing acoustic droplet ejection (ADE) methods to accurately and gently transfer small protein crystals (roughly 10 μm on each side) within microdroplets of mother liquor from the crystallization well, through a short air column (1−10 cm), to a standard X-ray diffraction mounting mesh. The acoustic droplet ejection instrumentation uses sound energy to transfer nanoliter to picoliter volumes from the surface of liquids. The principle that sound waves of great intensity near the surface of a liquid will eject droplets was demonstrated in 1927.[9] If sufficient energy from the transducer is focused near the surface, then a controlled ejection occurs. This is because the sound waves carry energy from a transducer to the focal point, where it produces a displacement of the surface that ejects a small droplet (Figure 1A). Potential energy transfers from a periodic compression wave to kinetic energy of an ejected particle. The wavelength of the sound governs the volume into which the energy is deposited.[10,11] Therefore, the ejected droplet diameter is proportional to the wavelength; consequently, smaller volume droplets are produced by higher-frequency (shorter wavelength) sound waves. The proportionality also yields very accurate ejected volumes (σ < 4%) that scale to 12 μm in diameter (1 pL in volume) or less.[10,12] If the hydrodynamic characteristics of the fluid are suitable and the sound wave is well focused, then the initial velocity of the ejected droplet is proportional to the amplitude of the focused wave.[13] Consequently, the transfer momentum of the droplet over a range of destination distances can be precisely controlled.

We and others have shown that ADE can rapidly transfer variable volumes of virtually any liquid with very high precision.[11,14] Consequently, it is ideal for many applications, including drug discovery.[15] However, ADE must not impact the crystal lattice and consequently its diffraction quality, which is inherently more fragile than covalent bonds. Indeed, ADE has been used very recently for seeding protein crystallization trials,[16] but to the best of our knowledge, not for X-ray diffraction and structure determination. Here, we report that ADE methods are well-suited for transferring 2.5 nL droplets of microcrystal slurries of insulin or lysozyme from a 384-well plate to standard MiTeGen (Ithaca, NY) micromesh mounting pins. After cryocooling, the micrometer-sized crystals are located on the mesh with the X-ray beam via a raster-scan strategy by the presence or absence of diffraction. Once microcrystals are located, partial data sets are collected and crystal structures determined to better than 2 Å resolution from merged data sets. Importantly, high-resolution structures can be determined from slurries of microcrystals that traditionally would have been discarded.

Received: April 13, 2011
Published: May 04, 2011

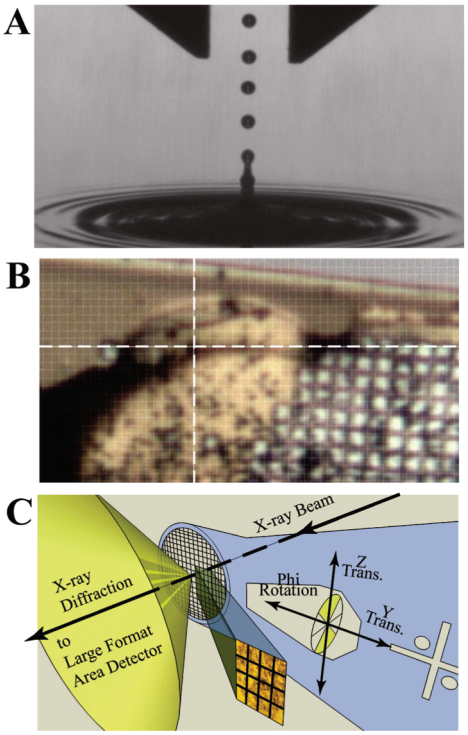

Figure 1. Concepts of ADE and raster-scanning. (A) Stroboscopic photomicrograph of a single 2.5 nL water droplet (~175 μm in diameter) launched via ADE from the liquid surface. The 1 mm width of the calipers at the top and the 400 ms strobe frequency are shown only to provide calibration. (B) Image from beamline X25 of the NSLS of the insulin microcrystal slurry supported on a micromesh (25 μm × 25 μm grid pattern) used to determine the structure. The 20 μm × 20 μm X-ray beam is centered at the intersection of the white cross hairs. (C) Illustration of the concepts for the raster-scanning X-ray diffraction strategy with a microdiffractometer and a several-micrometer wide X-ray beam (see also section 3 of the Supporting Information).

We prepared slurries of *Sus scrofa* (pig) Zn^{2+} insulin or *Gallus gallus* (hen egg white) lysozyme microcrystals as detailed in the Supporting Information (see also Figures S2−S4). Briefly, rhombohedral insulin microcrystals (space group *R*3) were obtained under low-salt conditions when the temperature was slowly lowered from 313 to 293 K.[17] Prior to ADE transfer, the insulin crystal slurries were concentrated by mild centrifugation and excess mother liquor was removed until the volume of crystalline material to the total volume was ~50% for the 10 μm and 25% for the 20 μm microcrystals. Lysozyme microcrystals of tetragonal lattice (space group $P4_32_12$) in the 5−20 μm range were obtained at room temperature from a highly saturated solution with sodium chloride and constant agitation using a reciprocating rocker.[18] The lysozyme microcrystal slurries, in which ~10% of the total volume consists of crystalline material, were not concentrated and used as is for ADE transfer.

We used a modified Echo liquid handling system at the Labcyte facility (Sunnyvale, CA) to transfer slurries of microcrystals of insulin and lysozyme. Briefly, some of the characteristics important to crystallography include (i) *x*/*y* translation control for both the source and the destination plate, (ii) two on-axis optical visualization cameras, and (iii) an off-axis optical stroboscopic system. We typically transferred one to four 2.5 nL droplets from a source well containing 100 μL of a slurry of microcrystals suspended in mother liquor augmented with cryosolvents to a MiTeGen 400/25 micromesh and then immediately plunged the mesh into liquid nitrogen to flash-cool the samples.

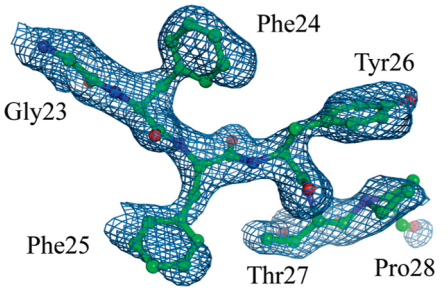

Figure 2. High-quality electron density maps obtained from ADE-mounted, serial microcrystallography. This experimental map, obtained from Zn SAD phases improved by solvent flattening (2.2 Å resolution, contoured at 1.5σ), was generated using data merged from nine different ADE-mounted insulin crystals. The interpretation of the map is consistent with two antiparallel β-strands assigned as B23−B28 (shown with C, N, and O atoms colored green, blue, and red, respectively) and D23−D28 (not shown).

X-ray diffraction data were collected at the NSLS and at the APS (Figure 1B, Table 1 and Table S1 of the Supporting Information). At each beamline, software designed for raster-scan searching (Figure 1C), X-ray diffraction image evaluation, and meta-data handling were used to find and collect X-ray diffraction data from the microcrystals.[19] Complete data sets were obtained by merging data from a small number of microcrystals (between 2 and 14) that were simultaneously ejected with one of the 2.5 nL droplets. Molecular replacement solutions were readily obtained for both insulin and lysozyme data using a polyalanine search model. The insulin crystals also yielded an anomalous signal in the data from two Zn^{2+} atoms located on the 3-fold symmetry axis. The small anomalous signal (~2.4%) and the phasing ambiguity that arises from anomalous scatterers located on a symmetry axis make insulin a challenging test case for SAD-based structure determination and have previously been used to evaluate new phasing methods.[20] The anomalous SAD data readily gave a correct heavy atom substructure. The initial maps obtained after density modification improvement of SAD phases from the 20 μm insulin crystals were clearly interpretable (Figure 2) and led to a high-quality SAD structure. All insulin structures determined from ADE transfer microcrystals revealed intact disulfide bridges (Figure S1 of the Supporting Information) indicating that the microcrystals had not experienced significant X-ray-induced radiation damage. We conclude that the diffraction quality of microcrystals is not appreciably impacted by the sound waves inherent to ADE methods or other forces encountered during droplet capture and cryocooling.

The X-ray brilliance and flux at new third-generation synchrotrons and X-ray FELs provide an opportunity to collect full diffraction data sets in ≪1 s. Advances in technology and automation are required to support high-throughput use of micrometer-sized crystals to fully exploit these X-ray sources. Our results demonstrate the feasibility of using ADE and raster-scanning strategies in microcrystallography at sources like NSLS-II. Moreover, by matching the frequency of the incident sound wave to the size of the crystals within the slurry, we are able to mount a single microcrystal with minimal solvent. This is critical for obtaining the signal to background noise ratio that is essential for determining structures from microcrystals. Therefore, ADE provides solutions to several challenges that must be overcome

Table 1. Data Collection and Model Refinement Statistics

	insulin (10 μm)	insulin (20 μm)	lysozyme (20 μm)
X-ray Diffraction Data Collection			
no. of crystals	14	9	2
X-ray source	NSLS X25	NSLS X25	APS 23ID-D
wavelength (Å)	1.280	1.280	0.9733
beam size (μm)	20 × 20	20 × 20	10 × 10
resolution (Å)	50−1.9	50−1.8	30−1.8
R_{sym} or R_{merge}	24.0 (39.6) [a]	11.4 (61.6) [a]	10.9 (36.7) [a]
$I/\sigma I$	46.4 (3.4) [a]	62.2 (2.1) [a]	16.9 (1.2) [a]
completeness (%)	93.5 (58.7) [a]	99.8 (96.7) [a]	94.9 (62.5) [a]
redundancy	6.5	10.5	1.8
Model Refinement			
no. of reflections	5917	7398	10280
R_{work}/R_{free}	16.7/20.3	18.1/22.3	16.8/21.2
rms deviations			
bond lengths (Å)	0.025	0.025	0.021
bond angles (deg)	2.244	2.159	1.938

[a] Data for the highest-resolution shell.

to realize the full potential of modern third-generation synchrotron sources and FELs.

■ ASSOCIATED CONTENT

Supporting Information. Sections describing insulin and lysozyme microcrystal preparations, crystal screening software, phasing and model refinement, ADE transfer of microcrystals, Table S1, and Figures S1−S4. This material is available free of charge via the Internet at http://pubs.acs.org.

Accession Codes

Atomic coordinates for the insulin structure determined using anomalous data and the corresponding structure factors have been deposited in the Protein Data Bank as entry 3RTO.

■ AUTHOR INFORMATION

Corresponding Author

*A.S.S.: phone, (631) 344-7306; fax, (631) 344-2741; e-mail, soares@bnl.gov. M.A.: phone, (631) 344-4795; fax, (631) 344-3238; e-mail, allaire@bnl.gov. A.M.O.: phone, (631) 344-4739; fax, (631) 344-2741; e-mail, amorv@bnl.gov.

Funding Sources

This work was supported by the Brookhaven National Laboratory/U.S. Department of Energy, Laboratory Directed Research and Development Grants 08-022 to A.M.O. and 11-008 to A.S.S. Additional support was provided by the Office of Biological and Environmental Research, U.S. Department of Energy, the National Center for Research Resources (Grant 2 P41 RR012408 to A.S.S., J.M.S., and A.M.O.), and the National Institute of General Medical Sciences (Grant Y1 GM 0080-03 to M.A.).

■ ACKNOWLEDGMENT

Insulin crystal data were measured at beamline X25 of the National Synchrotron Light Source (NSLS) at the Brookhaven National Laboratory. We thank Annie Héroux and the PXRR staff for numerous discussions. Use of the NSLS was supported by the U.S. Department of Energy Office of Basic Energy Sciences, under Contract DE-AC02-98CH10886. Lysozyme crystal data were measured at beamline 23ID-D of the Advanced Photon Source (APS) at Argonne National Laboratory (Argonne, IL). We thank Derek Yoder and the GMCA staff for their support. GM/CA CAT was funded in whole or in part with Federal funds from the National Cancer Institute (Y1-CO-1020) and the National Institute of General Medical Sciences (Y1-GM-1104). Use of the Advanced Photon Source was supported by the U.S. Department of Energy, Basic Energy Sciences, Office of Science, under Contract DE-AC02-06CH11357.

■ REFERENCES

(1) Seibert, M. M., Ekeberg, T., Maia, F. R., Svenda, M., Andreasson, J., Jonsson, O., Odic, D., Iwan, B., Rocker, A., and Westphal, D., et al. (2011) *Nature 470*, 78–81.

(2) Chapman, H. N., Fromme, P., Barty, A., White, T. A., Kirian, R. A., Aquila, A., Hunter, M. S., Schulz, J., DePonte, D. P., and Weierstall, U., et al. (2011) *Nature 470*, 73–77.

(3) Sawaya, M. R., Sambashivan, S., Nelson, R., Ivanova, M. I., Sievers, S. A., Apostol, M. I., Thompson, M. J., Balbirnie, M., Wiltzius, J. J., and McFarlane, H. T., et al. (2007) *Nature 447*, 453–457.

(4) Rasmussen, S. G., Choi, H. J., Rosenbaum, D. M., Kobilka, T. S., Thian, F. S., Edwards, P. C., Burghammer, M., Ratnala, V. R., Sanishvili, R., and Fischetti, R. F., et al. (2007) *Nature 450*, 383–387.

(5) Cherezov, V., Rosenbaum, D. M., Hanson, M. A., Rasmussen, S. G., Thian, F. S., Kobilka, T. S., Choi, H. J., Kuhn, P., Weis, W. I., and Kobilka, B. K., et al. (2007) *Science 318*, 1258–1265.

(6) Kirian, R. A., Wang, X., Weierstall, U., Schmidt, K. E., Spence, J. C., Hunter, M., Fromme, P., White, T., Chapman, H. N., and Holton, J. (2010) *Opt. Express 18*, 5713–5723.

(7) Ozaki, S., Bengtsson, J., Kramer, S. L., Krinsky, S., and Litvinenko, V. N. (2007) Philosophy for NSLS-II design with sub-nanometer horizontal emittance. In *Particle Accelerator Conference, PAC*, pp 77−79, IEEE, Piscataway, NJ.

(8) Hodgson, K. O., Anderson, W. F., Berman, L., Fischetti, R., et al. (2009) Workshop of the NIH Center for Research Resources and the National Institute of General Medical Sciences on Plans for Support of Future Life Science Synchrotron Research at NSLS-II, pp 1−14, National Institutes of Health, Bethesda, MD.

(9) Wood, E. W., and Loomis, A. L. (1927) Philosophical Magazine Series 7, Vol. 4, pp 417−436.

(10) Elrod, S. A., Hadimioglu, B., Khuri, X., Yakub, B. T., Rawson, E. G., Richley, E., Quate, C. F., Mansour, N. N., and Lundgren, T. S. (1989) *J. Appl. Phys. 65*, 3441–3447.

(11) Ellson, R., Mutz, M., Browning, B., Lee, L., Miller, M. F., and Papen, R. (2003) *J. Assoc. Lab. Automation 8*, 29–34.

(12) Comley, J. (2004) *Drug Discovery World Summer* 43–54.

(13) Stearns, R. G., and Ellson, R. N. (2002) Acoustic ejection of fluids using large F-number focusing elements. U.S. patent 6,416,164, Picoliter Inc., Mountain View, CA.

(14) David, H., Mitchell, M., Maria, S., Richard, S., Jean, S., Siobhan, P., Richard, E., and Joe, O. (2008) *J. Assoc. Lab. Automation 13*, 97–102.

(15) Ellson, R. (2002) *Drug Discovery Today 7*, S32–S34.

(16) Villaseñor, A. G., Wong, A., Shao, A., Garg, A., Kuglstatter, A., and Harris, S. F. (2010) *Acta Crystallogr. D66*, 568–576.

(17) Soares, A. S., Caspar, D. L., Weckert, E., Heroux, A., Holzer, K., Schroer, K., Zellner, J., Schneider, D., Nolan, W., and Sweet, R. M. (2003) *Acta Crystallogr. D59*, 1716–1724.

(18) Allaire, M., Moiseeva, N., Botez, C. E., Engel, M. A., and Stephens, P. W. (2009) *Acta Crystallogr. D65*, 379–382.

(19) Cherezov, V., Hanson, M. A., Griffith, M. T., Hilgart, M. C., Sanishvili, R., Nagarajan, V., Stepanov, S., Fischetti, R. F., Kuhn, P., and Stevens, R. C. (2009) *J. R. Soc., Interface 6*, S587–S597.

(20) Dauter, Z., Dauter, M., and Dodson, E. (2002) *Acta Crystallogr. D58*, 494–506.